

1 **How are under ice phytoplankton related to sea ice in**
2 **the Southern Ocean?**

3 **K. M Bisson¹, B. B. Cael²**

4 ¹Oregon State University, Corvallis, OR, USA
5 ²National Oceanography Centre, Southampton, UK

6 **Key Points:**

- 7 • Freeboard (ICESat-2) and under-ice plankton profiles (biogeochemical Argo floats)
8 are compared via their probability distributions.
9 • Freeboard variance, but not mean, is correlated to mean backscattering and chloro-
10 phyll maxima and the depths of these.
11 • Freeboard may influence plankton via modulation of light penetration, mixed layer
12 depth, and sea ice leads.

Abstract

Little is known about Southern Ocean under-ice phytoplankton, despite their suspected potential – ice and stratification conditions permitting – to produce blooms. We use a distributional approach to ask how Southern Ocean sea ice and under-ice phytoplankton characteristics are related, circumventing the dearth of co-located ice and phytoplankton data. We leverage all available Argo float profiles, together with freeboard (height of sea ice above sea level) and lead (ice fractures yielding open water) data from ICESat-2, to describe co-variations over time. We calculate moments of the probability distributions of maximum chlorophyll, particulate backscatter, the depths of these maxima, freeboard, and ice thickness. Argo moments correlate significantly with freeboard variance, lead fraction, and mixed layer depth, implying that sea ice dynamics drive plankton by modulating how much light they receive. We discuss ecological implications in the context of data limitations, and advocate for diagnostic models and field studies to test additional processes influencing under-ice phytoplankton.

Plain Language Summary

While sea ice undoubtedly influences under ice phytoplankton to some extent, little is known about under-ice phytoplankton in the Southern Ocean due to the paucity of field data. In the absence of plankton and ice measurements made at the same time and place, we can make inferences about the potential links between the two by comparing the average and variability of many measurements made within the same region. We do so with satellite-based measurements of freeboard (the thickness of sea ice above the water level) versus measurements made from profiling floats that measure plankton characteristics. We find that average freeboard is unrelated to these plankton measures but that when freeboard is more variable, phytoplankton stocks tend to be higher and occur at shallower depths. These nonintuitive results encapsulate how plankton communities' response to light is complex, and suggest that plankton may respond positively to a more variable light field.

1 Introduction

Earth's polar regions are extreme ecosystems, marked by perennial darkness and seasonal mosaics of sea ice that modify the salinity, temperature, and incoming light of subsurface waters. Recent work in the Arctic has shown that phytoplankton can thrive underneath sea ice, dwarfing previous estimates for phytoplankton productivity across the annual cycle (Arrigo et al., 2012, 2014; Assmy et al., 2017), and raising questions of how sea ice influences under ice phytoplankton.

The effects of sea ice on phytoplankton in the Southern Ocean remains largely unknown as much research has focused on the Arctic Ocean, although more recent studies have expressed the possibility of widespread microbial life under Antarctic sea ice from observations (Hague & Vichi, 2021; Arteaga et al., 2020; Cimoli et al., 2020). Phytoplankton in the Southern Ocean are primarily limited by light and iron, and massive blooms under ice sea are generally not suspected in this region. However, nutrient replenishment from deeper Winter mixed layer depths combined with light at the onset of Spring may enable phytoplankton growth under ice. Still needed are assessments of how ice characteristics affect the under ice environment. On one hand, the thicker snow cover of Southern Ocean sea ice compared to the Arctic may prohibit the transmission of light to the waters below because snow has a higher albedo than sea ice. On the other hand, most Antarctic sea ice melts in the Austral Spring and Summer (Pfirman et al., 1990), which may create a stable mixed layer and enhance growth of an already active under ice phytoplankton population previously living in deeper mixed layers (Hague & Vichi, 2021; A. A. Petty et al., 2014).

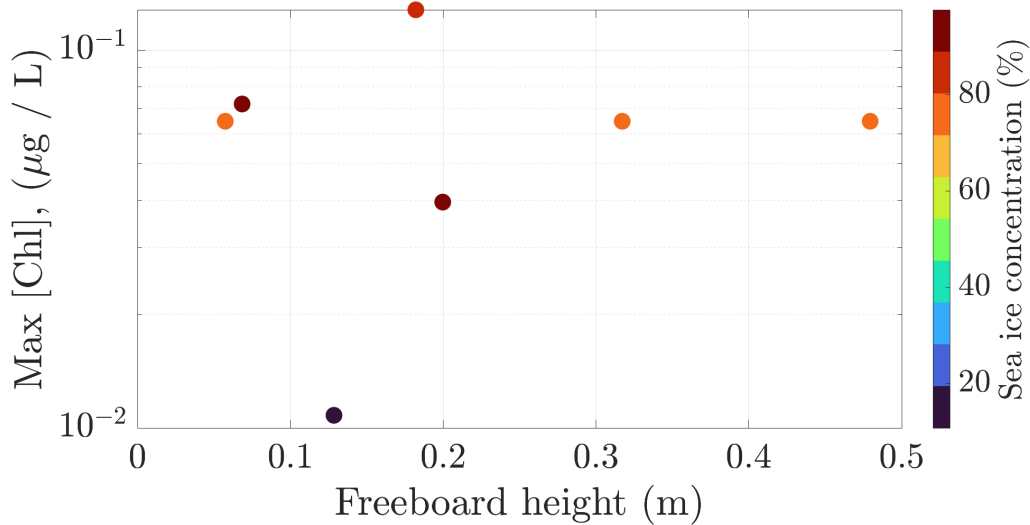


Figure 1. Maximum chlorophyll concentration of each under ice Argo profile is plotted against the same day freeboard from ICESat-2’s ATL10 product, matched within a 25km radius and colored by daily sea ice concentration values at a 25 x 25 km grid spacing. The Argo floats used in this plot are numbered ‘5904767,’ ‘5905995,’ and ‘5905102.’

62 Antarctic sea ice extent has increased in recent decades (Holland, 2014; Maksym
 63 et al., 2012) (although this trend has reversed in recent years), and the Southern Ocean
 64 is predicted to experience enhanced precipitation (Emori & Brown, 2005; Vignon et al.,
 65 2021) in the coming years which will affect snow on sea ice processes (e.g., sea ice flood-
 66 ing as well as sea ice thinning via insulation (Jacobs & Comiso, 1993)), all of which will
 67 influence sea ice thickness and albedo to some extent (Maksym & Markus, 2008; Arrigo
 68 et al., 2014). Aside from physical processes, sea ice also directly influences the biogeo-
 69 chemistry of the water column (Tagliabue & Arrigo, 2006) and potential for phytoplank-
 70 ton growth, supplying up to 70% of the daily iron flux during melting periods (Lannuzel
 71 et al., 2007; Wang et al., 2014). As phytoplankton form the base of the marine ecosys-
 72 tem and as polar regions will continue to be modified by climate change, it is critical to
 73 document any relationships between phytoplankton and sea ice now, in order to both
 74 describe current conditions and to motivate future research directions.

75 Ideally, mechanistic relationships between sea ice and phytoplankton would be quan-
 76 tified using numerous coupled direct sea ice - phytoplankton observations from field cam-
 77 paigns spanning season and location to capture a spectrum in sea ice thickness, nutri-
 78 ent, and light limitations. Unfortunately the scarcity of field measurements in the South-
 79 ern Ocean severely limits any such investigation currently. Instead, remote observations
 80 from either underwater profiling floats (such as the Argo program (Roemmich et al., 2009;
 81 Bittig et al., 2019)) or lidar satellites (e.g. ICESat-2 (Markus et al., 2017)) greatly im-

82 prove our ability to observe sea ice and water column properties during all times of the
 83 year. However, despite abundant remote observations from satellite and autonomous un-
 84 derwater floats, there are still very few same-day matchups of under ice phytoplankton
 85 and sea ice characteristics. As an illustration of this data paucity we plot the maximum
 86 chlorophyll concentration ([Chl], a pigment common to all phytoplankton) in the sur-
 87 face of an under ice float against the freeboard (height of sea ice above the sea surface),
 88 with ancillary information from daily sea ice concentration (Figure 1), totalling just 7
 89 observations of 1020 total, or less than 1% of available observations. All points shown
 90 are within a radius of 25km (a liberal range, given the phytoplankton decorrelation length-
 91 scales in the Southern Ocean of 10-15km (Haëntjens et al., 2017; Bisson et al., 2020)).
 92 Given that under ice [Chl], sea ice concentration, and freeboard are uncoupled in space
 93 and time, sea ice paired within 25km of an under ice float profile may not share the same
 94 water mass, and variable sea ice features (i.e. deformation, ridges, leads) will adjust the
 95 under ice light environment in ways not explicitly accounted for this type of match-up
 96 comparison. Clearly, a paired-observation style analysis severely reduces the amount of
 97 available data, and consequently reduces the questions that can be addressed regarding
 98 sea ice and phytoplankton.

99 While there are issues associated with using paired sea ice - phytoplankton data,
 100 it is plausible to expect some relationship between under ice biology and sea ice char-
 101 acteristics because sea ice influences light availability and mixed layer depths as men-
 102 tioned above (see also Behrenfeld et al. (2017), Arteaga et al. (2020), and Behera et al.
 103 (2020)). In this study we employ a distributional approach to leverage all available un-
 104 der ice observations during the same time period as the ICESat-2 satellite. The advan-
 105 tage of a distributional approach is to relate the quantities of interest via their proba-
 106 bility distributions' moments rather than on a point -per-point basis, and ultimately to
 107 learn how one underlying distribution may affect the other on broad scales of space and
 108 time. Distributional approaches have been used to identify new versus old ice apparent
 109 in the bimodal distributions of Arctic sea ice's total freeboard (e.g. (Kwok et al., 2019)),
 110 and these approaches have also been used to overcome data sparsity in linking ocean bi-
 111 ological measurements across scales (Cael et al., 2018, 2021). Our aim here is to describe
 112 the variability of the under ice biological environment (via changes in the chlorophyll con-
 113 centration and particulate backscattering, b_{bp} , which is known to covary with phytoplank-
 114 ton carbon) and to identify areas for future research.

115 2 Materials and Methods

116 2.1 Under Ice Argo Floats

117 Vertical under ice profiles of particulate backscattering (b_{bp} , m^{-1} , 700 nm hereafter
 118 referred to as b_{bp}) and adjusted chlorophyll concentration ([Chl], $ug L^{-1}$) were acquired
 119 from the Southern Ocean Carbon and Climate Observations and Modeling Project (SOC-
 120 COM). As in Bisson et al. (2019), profiles were despiked with a 3 point moving median
 121 to remove contamination from bubbles and/or the presence of rare, large non-algal par-
 122 ticles. Under ice Argo profiles are flagged from an ice avoidant algorithm, which forces
 123 a float to retreat from its ascent if the median of the seven near surface (20-50m depth)
 124 temperatures is less than -1.78 °C (Klatt et al., 2007). We removed profiles with sea ice
 125 concentration $< 15\%$ (via satellite data, see Supporting Information) to be consistent
 126 with the ICESat-2 freeboard processing.

127 We also calculate mixed layer depth (MLD, see Supporting Information) for each
 128 float based on the density gradient method (Dong et al., 2008). The MLD is thought to
 129 exert a large control on phytoplankton growth based on both bottom-up processes (light
 130 and nutrients) as well as the concentration of phytoplankton exposed to grazing pres-
 131 sure (Arteaga et al., 2020; Behrenfeld et al., 2013). We also compare Argo characteris-
 132 tics with the mean temperature within the MLD, as temperature is known to affect pho-

133 tosynthetic rates (Eppley, 1972). Altogether we note that the surface structure of un-
 134 der ice profiles is incomplete (due to missing surface data), and therefore our derived MLD
 135 are an imperfect approximation of the true MLD that may be achievable if the full pro-
 136 file were available. In total we have 1020 independent profiles across the shared time pe-
 137 riod of November 2018 to October 2020 where ATL20 data are available (more details
 138 in Supporting Information). Note we do not include under ice Argo data from January
 139 to March, as sea ice extent is minimal during these times and there are only several Argo
 140 profiles available. Otherwise, the median number of Argo profiles available per given month
 141 and year is 51, with a range of 16 to 79 observations.

142 Rather than e.g., calculating the median [Chl] and b_{bp} values within the mixed layer
 143 or euphotic depth (Bisson et al., 2019), we characterize under ice phytoplankton by re-
 144 porting the maximum [Chl] and b_{bp} values within a profile as well as the depth at which
 145 a maximum is found. Deeper [Chl] maxima that do not co-occur with the maxima of b_{bp}
 146 may imply changes due to photoacclimation rather than enhanced biomass. In our dataset,
 147 there are zero instances where the depth of maximum [Chl] or b_{bp} (hereafter z_c, z_b) is
 148 the shallowest depth in the profile, which suggests the reported z_c or z_b value is likely
 149 a good approximation of the true z_c or z_b value. One notable exception is if there are
 150 biomass peaks in the near surface (1-5m) waters that are not captured with the floats,
 151 which can be the case for ice algae sloughing from the ice bottom from melting ice (Ardyna
 152 et al., 2020).

153 2.2 Sea Ice Data Products

154 We acquire total freeboard from ICESat-2 (Ice, Cloud, and land Elevation Satel-
 155 lite), distributed via the National Snow and Ice Data Center (NSIDC) and downloaded
 156 using Icepyx (Scheick et al., 2019, 2019–). ICESat-2 was launched in October 2018 with
 157 the primary goal of quantifying cryosphere and terrestrial elevations with extremely high
 158 precision never before achieved from spacecraft (Markus et al., 2017). The primary in-
 159 strument aboard ICESat-2 is ATLAS (Advanced Topographic Laser Altimeter System),
 160 which is a lidar that generates roughly 10,000 laser pulses per second and converts the
 161 time it takes for a small fraction of photons to return into a distance, and ultimately into
 162 a surface height. In this study we use the ATL07, ATL10, and ATL20 products.

163 Sea ice types are provided in ATL07 (Kwok et al., 2021b) and are used to compute
 164 the fraction of sea ice segments that are leads relative to the total segment length. While
 165 ICESat-2 delivers ungridded data in along-track granules, over the course of a month,
 166 the along-track segments approximate a 2D field (see Horvat et al. (2020)). In this study
 167 we use the specular lead (i.e., narrow gaps and fractures within the ice and between ice
 168 floes, (A. Petty et al., 2021) identification, which is determined from an empirical de-
 169 cision tree. ATL10 data (Kwok et al., 2021a) provide same day freeboard for under ice
 170 Argo data shown in Figure 1. The ATL20 product (A. A. Petty et al., 2021) provides
 171 monthly means of freeboard (m) in 25 x 25km pixels. Freeboard is determined from leads
 172 (which provide a reference sea surface height) along each beam from the ATL07 photon
 173 height product, and the data do not include cloudy conditions or when daily sea ice con-
 174 centration < 15%. Only the strong beams were used in analysis, and we use ICESat-2
 175 products from October 2018 until October 2020.

176 Total freeboard (F , hereafter F from the ATL20 product) is the sum of sea ice and
 177 snow present above the ocean’s surface. The total sea ice thickness (I , meters) will vary
 178 depending on the ratio sea ice ice thickness to snow depth, or R . We calculate sea ice
 179 thickness in addition to F , where R values are calculated dynamically from F depend-
 180 ing on the location of the sea ice (Li et al., 2018). We note that we choose to show our
 181 results using F rather than I due to the assumptions and error in calculating I , but choos-
 182 ing I rather than F did not change our results. Finally, daily gridded (25x25km) sea ice
 183 concentration data were downloaded for the same day paired ATL10-Argo data shown

184 in Figure 1. Argo and sea ice data were aggregated into unique year-month bins to fac-
 185 facilitate comparison between both classes of data. We use these broad space/time con-
 186 straints due to the location uncertainty in under ice floats as well as temporal resolu-
 187 tion differences between Argo and ice data (which do not permit a point-by-point ex-
 188 amination). We take Argo observations within a given month to be representative of that
 189 month, due to good spatial coverage of the Southern Ocean (See Supporting Informa-
 190 tion).

191 2.3 Statistical framework

192 The complexity underlying the distributions of F , I , b_{bp} , $[Chl]$, z_c , and z_b is dis-
 193 tilled and described through the first three moments of each distribution: the mean, vari-
 194 ance, and skewness. While the mean and variance describe the average and spread of the
 195 data, skewness quantifies how lopsided a distribution is relative to a perfectly symmet-
 196 rical distribution (i.e., a positively skewed distribution has a heavier tail on the right side,
 197 meaning the mean exceeds the median). We calculate the mean, variance, and skewness
 198 for each distribution (i.e. b_{bp} , $[Chl]$, z_b , z_c , F , I) for each unique month and year when
 199 data are available. Both b_{bp} and $[Chl]$ are logarithmically distributed (i.e. span a large
 200 dynamic range) so we calculate their moments of the log-transformed variables. The strength
 201 of any relationships between variables is assessed through Kendall’s τ , a non-parametric
 202 rank correlation.

203 We note that while b_{bp} and $[Chl]$ both covary with phytoplankton biomass, neither
 204 variable perfectly quantifies phytoplankton. Although b_{bp} has better performance met-
 205 rics with phytoplankton carbon compared to chlorophyll (see Graff et al. (2015)), b_{bp} is
 206 imperfect as it also covaries with non-algal particles. For most of the year, the major-
 207 ity of particles under the ice will be phytoplankton, but there may be times in the Aus-
 208 tral summer (e.g., export of fecal material and cell aggregates, (Moreau et al., 2020)) when
 209 a portion of particles are non-algal. On the other hand, $[Chl]$ is found in all phytoplank-
 210 ton, but it is plastic and varies with the light field. A change in $[Chl]$ does not necessar-
 211 ily imply a change in biomass because cells can modify their pigment concentration ac-
 212 cording to irradiance levels. Both quantities are useful to assess phytoplankton under
 213 ice, and b_{bp} might be useful for assessing particles under ice for times of the year when
 214 particles are expected.

215 3 Temporal Patterns in under ice properties

216 Distributions of b_{bp} and $[Chl]$ show clear seasonality for the month and year pair-
 217 ings when all data are available (Figure 2). The maximum F occurs in December and
 218 there are subtle shifts in the width of F throughout the annual cycle, with June and July
 219 representing the least variable F distributions in both 2019 and 2020.

220 The shapes of maximum b_{bp} vary tremendously from month to month across the
 221 annual cycle, with long tails of b_{bp} in October - December, and shorter tails in June and
 222 July. There are times of the year when the distribution of b_{bp} is unimodal, and other times
 223 when its roughly bimodal (e.g., December 2018, May 2019, September - December 2019,
 224 August - September 2020). Like b_{bp} , $[Chl]$ distributions tend to have longer tails from
 225 October - December, but unlike b_{bp} , $[Chl]$ distributions tend to be left-skewed from April
 226 to June. In general $[Chl]$ has wider distributions throughout the annual cycle compared
 227 to b_{bp} .

228 The seasonal cycle in b_{bp} and $[Chl]$ is more pronounced than that of F or z_b and
 229 z_c . Previous work found that under ice phytoplankton growth initiates before melting
 230 (Hague & Vichi, 2021), and also that phytoplankton can grow under low light conditions
 231 compared to what was previously thought in the Antarctic (Arteaga et al., 2020)). Our
 232 work is in broad agreement with these studies, especially as there are longer tails in the

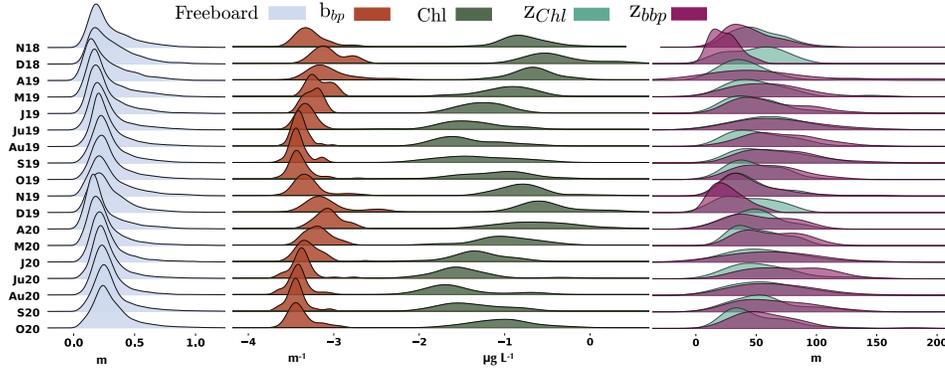


Figure 2. Ridge plot comparing probability density functions of F (grey, left), b_{bp} (orange, log10 transformed), $[Chl]$ (green, log10 transformed), z_c (teal), and z_b (purple) across month (y-axis). Note that Jan-March are not shown and are not included in analyses because there are too few Argo observations in those months.

233 distribution of b_{bp} and $[Chl]$ from August through September, implying more instances
 234 of anomalously high biomass.

235 What differences in the distributions of sea ice and phytoplankton characteristics
 236 might be expected? For example, b_{bp} or $[Chl]$ reflect a balance between phytoplankton
 237 growth and losses, ultimately depending on the light and nutrient environment as well
 238 as viral activity and grazing pressure. Photoacclimation and physical mixing in the wa-
 239 ter column influence z_b and z_c , including algae released into waters from the base of melt-
 240 ing sea ice (Yoshida et al., 2020). One might expect enhanced b_{bp} and $[Chl]$ with decreas-
 241 ing $\mu(F)$ and $\mu(I)$ if phytoplankton are primarily light limited. If algae living in sea ice
 242 are a dominant control on variability in z_b or z_c , we expect z_b and z_c will shoal in tan-
 243 dem with melting ice.

244 There are seasonal patterns in the distributions of z_b and z_c as well, where the mean
 245 z_b is usually much less than z_c during November and December, but z_b slightly exceeds
 246 z_c during Winter and Spring. The former might imply a flux of algae and their aggre-
 247 gates into the water from melting sea ice (Moreau et al., 2020), and/or possibly fecal pel-
 248 lets from krill feeding on algal ice populations at the near surface (Arrigo & Thomas,
 249 2004). We note that algal ice is expected to contribute a greater fraction of productiv-
 250 ity (relative to the in water phytoplankton) in October and November (Lizotte, 2001),
 251 so it is plausible that there could be enhanced export flux (i.e., higher particle loads, or
 252 enhanced $\mu(b_{bp})$ relative to $\mu([Chl])$ in November and December. A combination of slough-
 253 ing algae from sea ice, as well as export of particles (including senescent algal cells), might
 254 create bimodal distributions in b_{bp} , $[Chl]$, z_b and z_c , as is observed to different degrees
 255 from September through December.

256 4 Relating Distributions Through Their Moments

257 A distributional approach doesn't provide causal links between sea ice and phy-
 258 toplankton, but it is nevertheless useful to identify what the current data suggests. The
 259 Argo moments (in particular the mean, $\mu(\cdot)$) correlate moderately well with ice variance
 260 ($\sigma(\cdot)$) and ice skewness but not with ice mean (Figure 3). Both $\mu(b_{bp})$ and $\mu([Chl])$ in-
 261 crease with increasing ice variance, and $\mu(z_c)$ and $\mu(z_b)$ decrease with increasing $\sigma(F)$.
 262 In general, the Argo σ moments do not relate well to ice moments, with the exception
 263 of $\sigma(b_{bp})$, which is positively correlated with $\sigma(F)$. $\mu(z_b)$ increases with increasing ice

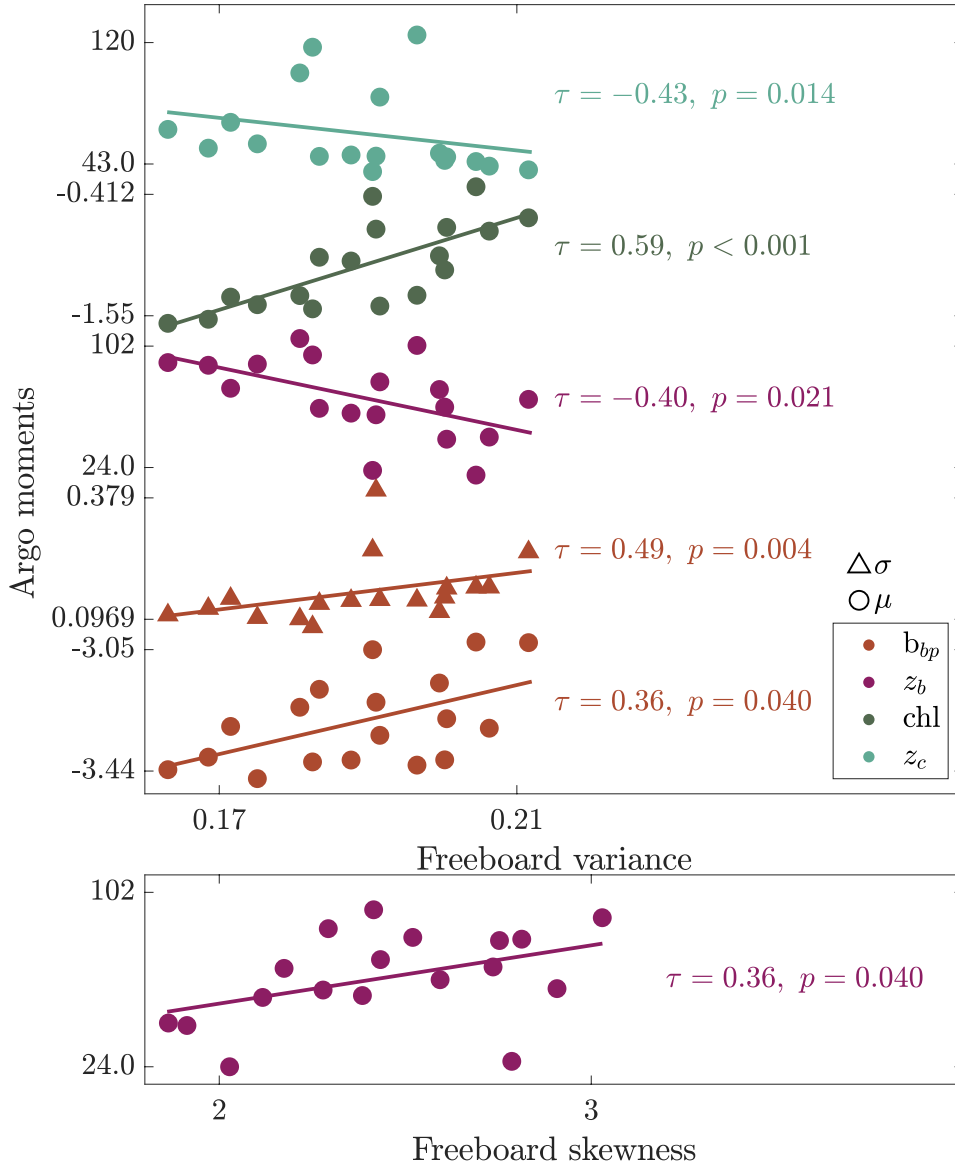


Figure 3. Trends in Argo moments and ice variance (top panel) as well as Argo z_b and ice skewness (bottom panel) across Argo variates (b_{bp} , [Chl], z_b and z_c). For top plot, separate y-ticks are given for each moment-variable combination to show their ranges. Note that b_{bp} and [Chl] are shown in log-scales, and all points are the monthly values.

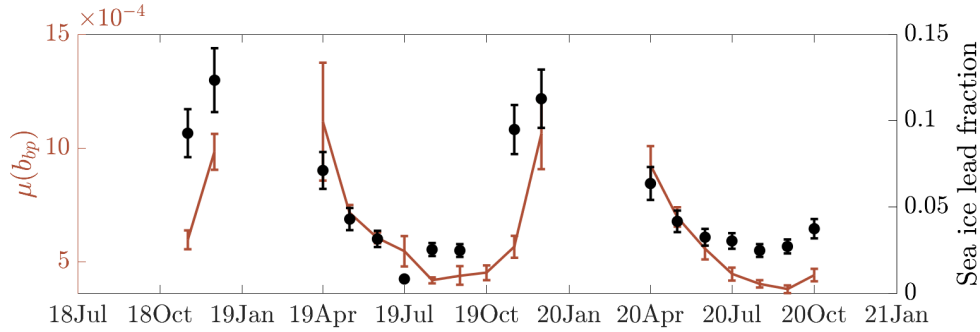


Figure 4. Time series of $\mu(b_{bp})$ (m^{-1}) using all available under ice Argo data and the sea ice lead fraction of specular leads (gaps and fractures between ice floes). Error bars represent the coefficient of variation for each month.

264 skewness. Put another way, a variable ice environment coincides with higher b_{bp} and [Chl]
 265 at shallower depths. Months with greater proportions of thicker ice have deeper depths
 266 of maximum b_{bp} . Neither $\mu(b_{bp})$ nor $\mu[\text{Chl}]$ are significantly correlated with statistical
 267 moments of temperature (p values exceed 0.1 in all cases, and generally exceed 0.5). MLD
 268 correlates most strongly and negatively with phytoplankton ($\mu(\text{MLD})$ and $\mu(b_{bp})$ have
 269 a τ of -0.73 and a p-value < 0.005, while $\mu(\text{MLD})$ and $\mu([\text{Chl}]$ have a τ of -0.54 and a
 270 p-value < 0.005), evincing that light exerts a strong control over phytoplankton in this
 271 study. We cannot assess the role of nutrients (and iron in particular) in this study due
 272 to lack of data, and therefore cannot say e.g., if iron versus sea ice and MLD has a stronger
 273 influence on phytoplankton under ice.

274 The presence of significant, moderate correlations between sea ice variance and Argo
 275 moments, as opposed to the weak correlations between sea ice mean and Argo moments,
 276 implies that variance in ice thickness is more influential than mean ice thickness for phy-
 277 toplankton growth. The negative relationship between ice variance and $\mu(z_b)$ is some-
 278 what counter intuitive, as one might expect z_b to become more variable as ice variance
 279 increases.

280 However, if the relationship between F and plankton characteristics is nonlinear,
 281 it is plausible that $\sigma(F)$ is what drives greater and shallower plankton stocks. Light trans-
 282 mission through sea ice is $\propto e^{-kF}$ (Beer's law) for a given k related to sea ice proper-
 283 ties. As light penetration decreases nonlinearly with ice thickness, there's a greater dif-
 284 ference in light transmission through F of e.g., 0 and 1m than between 1 and 2m, and
 285 so on as F increases. All other factors constant, average light penetration in a region is
 286 affected by how much of the total ice is sufficiently thin to permit light transmission, and
 287 by how thick ice is in this area - in other words, the low tail of F . The low tail of F
 288 is best captured by $\sigma(F)$ given that F is positively skewed, so ultimately, this low tail of
 289 small- F values can be what dominates total light penetration, and hence plankton char-
 290 acteristics.

291 Underlying the statistically significant relationships of sea ice, MLD, and phyto-
 292 plankton are possible mechanistic explanations. The near seasonality in b_{bp} and [Chl],
 293 coupled with the correlations of Argo moments to ice variance and leads implies leads
 294 and/or thin sea ice permit light to reach the phytoplankton at all times of the year to
 295 varying degrees (Figure 4). Indeed, the seasonal cycle of maximum b_{bp} tracks very well
 296 with the sea ice specular lead fraction (Figure 4, note that Spearman's rank correlation
 297 between lead fraction and $\mu(b_{bp})$ is 0.78, and $\tau = 0.58$), where higher specular lead frac-
 298 tions also coincide with greater incident photosynthetically active radiation in the South-
 299 ern Ocean and more shallow MLD. Under ice phytoplankton are mobile, embedded in

300 water masses transiting beneath both snow covered ice and brief exposure to open wa-
301 ter, and consequently are likely to experience intermittent pulses of light that they may
302 have adapted to use efficiently.

303 Our findings differ with those of the Lowry et al. (2018) study, which found that
304 leads inhibited phytoplankton blooms via convective mixing in the Arctic Ocean. In the
305 Southern Ocean, we found that a higher fraction of leads corresponds to larger maxima
306 in under ice [Chl] that occur at more shallow depths, which is most similar to the find-
307 ings of Assmy et al. (2017) in the Arctic Ocean. The magnitude of under ice [Chl] in the
308 Southern Ocean is generally less than that of Arctic blooms, but the magnitude of un-
309 der ice [Chl] in the Southern Ocean is comparable (at times exceeding) to that of the
310 ice-free areas of the Southern Ocean (Rembauville et al., 2017; Haëntjens et al., 2017)(i.e.,
311 in this study the maximum [Chl] is 8 μg per L).

312 5 Concluding remarks

313 We have employed a statistical approach as a way to overcome the shortage of data.
314 Although there are numerous measurements of either Argo or ICESat-2 observations by
315 themselves, there were no true paired observations between ICESat-2 and Argo. The in-
316 herent position uncertainty associated with under ice Argo floats almost certainly means
317 no exact match ups (i.e., those within reasonable space and time constraints) between
318 Argo and any other sensor can be expected in the future, unless under ice acoustic po-
319 sitioning can help decrease position uncertainty. Still, the continued presence of Argo
320 floats in the Southern Ocean will undoubtedly help to address the role of sea ice and phy-
321 toplankton growth. Ideally all SOCCOM Argo floats would be equipped with photosyn-
322 thetically active radiation sensors, unlike those used herein. While there were sufficient
323 profiles in this study to examine monthly distributions, we could not examine regional
324 differences due to the dataset size. In the coming years, more under ice data will become
325 available and perhaps permit such an analysis. Here we found enhanced phytoplankton
326 biomass and variability with decreasing MLD, increasing F variance, and increasing lead
327 fractions, which might plausibly be explained by factors not addressed in this study (i.e.,
328 spatial differences in iron availability and grazing pressure).

329 Despite the limitations, statistical approaches remain useful to understand general
330 patterns in under ice phytoplankton, and time series analyses will become important as
331 more data become available in the coming decades. In order to build a mechanistic un-
332 derstanding of phytoplankton under sea ice, synergistic models could incorporate data
333 from Argo with other platforms. Large scale climate modeling is also important for as-
334 sessing the likelihood of phytoplankton growth based on environmental conditions (e.g.,
335 ice cover, MLD) that might be informed from our findings here.

336 Neither models nor statistical methods replace field work. We recommend field stud-
337 ies incorporating under ice light, phytoplankton, and zooplankton in particular, as well
338 as measuring sea-ice algal communities, (Cimoli et al., 2017). Under ice phytoplankton
339 blooms have commonly been treated as the result of bottom-up processes (i.e., light and
340 nutrient status), and our study focused on ice and phytoplankton characteristics. More
341 Information about nutrient status, zooplankton (perhaps from the deployment of imag-
342 ing sensors, such as the Underwater Vision Profiler) and other heterotrophic activity would
343 help to more explicitly characterize the many mechanisms influencing phytoplankton un-
344 der sea ice beyond what has been considered here.

345 Acknowledgments

346 We are grateful to Ted Maksym, Emmanuel Boss, and Chris Horvat for helpful conver-
347 sations, to the Icepyx team (especially Jessica Scheick, Romina Piunno, and Rachel Till-
348 ing), and to the ICESat-2 science team and project office for their support. We thank

349 Sébastien Moreau and Emma Cavan for their help improving our manuscript. Argo data
 350 were collected and made freely available by the Southern Ocean Carbon and Climate Ob-
 351 servations and Modeling (SOCCOM) Project funded by the National Science Founda-
 352 tion, Division of Polar Programs (NSF PLR -1425989 and OPP-1936222), supplemented
 353 by NASA, and by the International Argo Program and the NOAA programs that con-
 354 tribute to it. (<https://soccomp.princeton.edu/www/index.html>). The Argo Program
 355 is part of the Global Ocean Observing System. ICESat-2 data can be accessed via <https://nsidc.org/data/atl07>.
 356 KB acknowledges NASA grant 80NSSC20K0970. BBC acknowledges support by the Na-
 357 tional Environmental Research Council Grant NE/T010622/1 CELOS (Constraining the
 358 EvoLution of the southern Ocean carbon Sink).

359 References

- 360 Ardyna, M., Mundy, C., Mayot, N., Matthes, L. C., Oziel, L., Horvat, C., ... others
 361 (2020). Under-ice phytoplankton blooms: Shedding light on the invisible part
 362 of arctic primary production. *Frontiers in Marine Science*, 7, 985.
- 363 Arrigo, K. R., Perovich, D. K., Pickart, R. S., Brown, Z. W., Van Dijken, G. L.,
 364 Lowry, K. E., ... others (2012). Massive phytoplankton blooms under arctic
 365 sea ice. *Science*, 336(6087), 1408–1408.
- 366 Arrigo, K. R., Perovich, D. K., Pickart, R. S., Brown, Z. W., van Dijken, G. L.,
 367 Lowry, K. E., ... others (2014). Phytoplankton blooms beneath the sea ice in
 368 the chukchi sea. *Deep Sea Research Part II: Topical Studies in Oceanography*,
 369 105, 1–16.
- 370 Arrigo, K. R., & Thomas, D. N. (2004). Large scale importance of sea ice biology in
 371 the southern ocean. *Antarctic Science*, 16(4), 471.
- 372 Arteaga, L. A., Boss, E., Behrenfeld, M. J., Westberry, T. K., & Sarmiento, J. L.
 373 (2020). Seasonal modulation of phytoplankton biomass in the southern ocean.
 374 *Nature communications*, 11(1), 1–10.
- 375 Assmy, P., Fernández-Méndez, M., Duarte, P., Meyer, A., Randelhoff, A., Mundy,
 376 C. J., ... others (2017). Leads in arctic pack ice enable early phytoplankton
 377 blooms below snow-covered sea ice. *Scientific reports*, 7(1), 1–9.
- 378 Behera, N., Swain, D., & Sil, S. (2020). Effect of antarctic sea ice on chlorophyll
 379 concentration in the southern ocean. *Deep Sea Research Part II: Topical Stud-
 380 ies in Oceanography*, 178, 104853.
- 381 Behrenfeld, M. J., Doney, S. C., Lima, I., Boss, E. S., & Siegel, D. A. (2013). An-
 382 nual cycles of ecological disturbance and recovery underlying the subarctic
 383 atlantic spring plankton bloom. *Global biogeochemical cycles*, 27(2), 526–540.
- 384 Behrenfeld, M. J., Hu, Y., OMalley, R. T., Boss, E. S., Hostetler, C. A., Siegel,
 385 D. A., ... others (2017). Annual boom–bust cycles of polar phytoplankton
 386 biomass revealed by space-based lidar. *Nature Geoscience*, 10(2), 118–122.
- 387 Bisson, K., Boss, E., Werdell, P., Ibrahim, A., & Behrenfeld, M. (2020). Particulate
 388 backscattering in the global ocean: A comparison of independent assessments.
 389 *Geophysical Research Letters*, e2020GL090909.
- 390 Bisson, K., Boss, E., Westberry, T., & Behrenfeld, M. (2019). Evaluating satellite
 391 estimates of particulate backscatter in the global open ocean using autonomous
 392 profiling floats. *Optics express*, 27(21), 30191–30203.
- 393 Bittig, H. C., Maurer, T. L., Plant, J. N., Schmechtig, C., Wong, A. P., Claustre, H.,
 394 ... others (2019). A bgc-argo guide: Planning, deployment, data handling and
 395 usage. *Frontiers in Marine Science*, 6, 502.
- 396 Cael, B., Bisson, K., Conte, M., Duret, M. T., Follett, C. L., Henson, S. A., ...
 397 others (2021). Open ocean particle flux variability from surface to seafloor.
 398 *Geophysical Research Letters*, 48(9), e2021GL092895.
- 399 Cael, B., Bisson, K., & Follett, C. L. (2018). Can rates of ocean primary production
 400 and biological carbon export be related through their probability distributions?
 401 *Global biogeochemical cycles*, 32(6), 954–970.

- 402 Cavalieri, D. (1996). *Nasa team sea ice algorithm*.
- 403 Cimoli, E., Lucieer, A., Meiners, K. M., Lund-Hansen, L. C., Kennedy, F., Mar-
404 tin, A., . . . Lucieer, V. (2017). Towards improved estimates of sea-ice algal
405 biomass: experimental assessment of hyperspectral imaging cameras for under-
406 ice studies. *Annals of Glaciology*, *58*(75pt1), 68–77.
- 407 Cimoli, E., Lucieer, V., Meiners, K. M., Chennu, A., Castrisios, K., Ryan, K. G.,
408 . . . Lucieer, A. (2020). Mapping the in situ microspatial distribution of ice
409 algal biomass through hyperspectral imaging of sea-ice cores. *Scientific reports*,
410 *10*(1), 1–17.
- 411 Dong, S., Sprintall, J., Gille, S. T., & Talley, L. (2008). Southern ocean mixed-
412 layer depth from argo float profiles. *Journal of Geophysical Research: Oceans*,
413 *113*(C6).
- 414 Emori, S., & Brown, S. (2005). Dynamic and thermodynamic changes in mean
415 and extreme precipitation under changed climate. *Geophysical Research Let-
416 ters*, *32*(17).
- 417 Eppley, R. W. (1972). Temperature and phytoplankton growth in the sea. *Fish. bull.*,
418 *70*(4), 1063–1085.
- 419 Graff, J. R., Westberry, T. K., Milligan, A. J., Brown, M. B., Dall’Omo, G., van
420 Dongen-Vogels, V., . . . Behrenfeld, M. J. (2015). Analytical phytoplankton
421 carbon measurements spanning diverse ecosystems. *Deep Sea Research Part I:
422 Oceanographic Research Papers*, *102*, 16–25.
- 423 Haëntjens, N., Boss, E., & Talley, L. D. (2017). Revisiting ocean color algorithms
424 for chlorophyll a and particulate organic carbon in the southern ocean us-
425 ing biogeochemical floats. *Journal of Geophysical Research: Oceans*, *122*(8),
426 6583–6593.
- 427 Hague, M., & Vichi, M. (2021). Southern ocean biogeochemical argo detect under-
428 ice phytoplankton growth before sea ice retreat. *Biogeosciences*, *18*(1), 25–38.
- 429 Holland, P. R. (2014). The seasonality of antarctic sea ice trends. *Geophysical Re-
430 search Letters*, *41*(12), 4230–4237.
- 431 Horvat, C., Blanchard-Wrigglesworth, E., & Petty, A. (2020). Observing waves in
432 sea ice with icesat-2. *Geophysical Research Letters*, *47*(10), e2020GL087629.
- 433 Jacobs, S. S., & Comiso, J. C. (1993). A recent sea-ice retreat west of the antarctic
434 peninsula. *Geophysical Research Letters*, *20*(12), 1171–1174.
- 435 Johnson, K. S., Plant, J. N., Coletti, L. J., Jannasch, H. W., Sakamoto, C. M.,
436 Riser, S. C., . . . others (2017). Biogeochemical sensor performance in the
437 soccom profiling float array. *Journal of Geophysical Research: Oceans*, *122*(8),
438 6416–6436.
- 439 Klatt, O., Boebel, O., & Fahrbach, E. (2007). A profiling floats sense of ice. *Journal
440 of Atmospheric and Oceanic Technology*, *24*(7), 1301–1308.
- 441 Kwok, R., Markus, T., Kurtz, N., Petty, A., Neumann, T., Farrell, S., . . . Wimert,
442 J. (2019). Surface height and sea ice freeboard of the arctic ocean from icesat-
443 2: Characteristics and early results. *Journal of Geophysical Research: Oceans*,
444 *124*(10), 6942–6959.
- 445 Kwok, R., Petty, A., Cunningham, G., Markus, T., Hancock, D., Ivanoff, A., . . . the
446 ICESat-2 Science Team (2021a). Atlas/icesat-2 l3a sea ice freeboard, version 4.
447 *Boulder, Colorado USA. NSIDC: National Snow and Ice Data Center*.
- 448 Kwok, R., Petty, A., Cunningham, G., Markus, T., Hancock, D., Ivanoff, A., . . . the
449 ICESat-2 Science Team (2021b). Atlas/icesat-2 l3a sea ice height, version 4.
450 *Boulder, Colorado USA. NSIDC: National Snow and Ice Data Center*.
- 451 Lannuzel, D., Schoemann, V., De Jong, J., Tison, J.-L., & Chou, L. (2007). Distri-
452 bution and biogeochemical behaviour of iron in the east antarctic sea ice. *Ma-
453 rine Chemistry*, *106*(1-2), 18–32.
- 454 Li, H., Xie, H., Kern, S., Wan, W., Ozsoy, B., Ackley, S., & Hong, Y. (2018). Spatio-
455 temporal variability of antarctic sea-ice thickness and volume obtained from
icesat data using an innovative algorithm. *Remote Sensing of Environment*,

- 219, 44–61.
- 457 Lizotte, M. P. (2001). The contributions of sea ice algae to antarctic marine primary
458 production. *American zoologist*, *41*(1), 57–73.
- 459 Lowry, K. E., Pickart, R. S., Selz, V., Mills, M. M., Pacini, A., Lewis, K. M., ...
460 others (2018). Under-ice phytoplankton blooms inhibited by spring convective
461 mixing in refreezing leads. *Journal of Geophysical Research: Oceans*, *123*(1),
462 90–109.
- 463 Maksym, T., & Markus, T. (2008). Antarctic sea ice thickness and snow-to-ice con-
464 version from atmospheric reanalysis and passive microwave snow depth. *Jour-
465 nal of Geophysical Research: Oceans*, *113*(C2).
- 466 Maksym, T., Stammerjohn, S. E., Ackley, S., & Massom, R. (2012). Antarctic sea
467 ice a polar opposite? *Oceanography*, *25*(3), 140–151.
- 468 Markus, T., Neumann, T., Martino, A., Abdalati, W., Brunt, K., Csatho, B., ...
469 others (2017). The ice, cloud, and land elevation satellite-2 (icesat-2): science
470 requirements, concept, and implementation. *Remote sensing of environment*,
471 *190*, 260–273.
- 472 Moreau, S., Boyd, P. W., & Strutton, P. G. (2020). Remote assessment of the fate
473 of phytoplankton in the southern ocean sea-ice zone. *Nature communications*,
474 *11*(1), 1–9.
- 475 Pellichero, V., Sallée, J.-B., Schmidtko, S., Roquet, F., & Charrassin, J.-B. (2017).
476 The ocean mixed layer under southern ocean sea-ice: Seasonal cycle and forc-
477 ing. *Journal of Geophysical Research: Oceans*, *122*(2), 1608–1633.
- 478 Petty, A., Bagnardi, M., Kurtz, N., Tilling, R., Fons, S., Armitage, T., ... Kwok, R.
479 (2021). Assessment of icesat-2 sea ice surface classification with sentinel-2 im-
480 agery: Implications for freeboard and new estimates of lead and floe geometry.
481 *Earth and Space Science*, *8*(3), e2020EA001491.
- 482 Petty, A. A., Holland, P. R., & Feltham, D. L. (2014). Sea ice and the ocean mixed
483 layer over the antarctic shelf seas. *The Cryosphere*, *8*(2), 761–783.
- 484 Petty, A. A., Kwok, R., Bagnardi, M., Ivanoff, A., Kurtz, N., Lee, J., ... Hancock,
485 D. (2021). Atlas/icesat-2 l3b daily and monthly gridded sea ice freeboard,
486 version 2. *Boulder, Colorado USA. NSIDC: National Snow and Ice Data
487 Center*.
- 488 Pfirman, S., Lange, M., Wollenburg, I., & Schlosser, P. (1990). Sea ice characteris-
489 tics and the role of sediment inclusions in deep-sea deposition: Arcticantarctic
490 comparisons. In *Geological history of the polar oceans: Arctic versus antarctic*
491 (pp. 187–211). Springer.
- 492 Rembauville, M., Briggs, N., Ardyna, M., Uitz, J., Catala, P., Penkerch, C., ...
493 Blain, S. (2017). Plankton assemblage estimated with bgc-argo floats in the
494 southern ocean: Implications for seasonal successions and particle export.
495 *Journal of Geophysical Research: Oceans*, *122*(10), 8278–8292.
- 496 Riser, S. C., Swift, D., & Drucker, R. (2018). Profiling floats in soccom: Technical
497 capabilities for studying the southern ocean. *Journal of Geophysical Research:
498 Oceans*, *123*(6), 4055–4073.
- 499 Roemmich, D., Johnson, G. C., Riser, S., Davis, R., Gilson, J., Owens, W. B., ...
500 Ignaszewski, M. (2009). The argo program: Observing the global ocean with
501 profiling floats. *Oceanography*, *22*(2), 34–43.
- 502 Scheick, J., Arendt, A., Heagy, L., & Perez, F. (2019). Introducing icepyx, an open
503 source python library for obtaining and working with icesat-2 data. *Earth and
504 Space Science Open Archive ESSOAr*.
- 505 Scheick, J., et al. (2019–). *icepyx: Python tools for obtaining and working with
506 ICESat-2 data*. Retrieved from <https://github.com/icesat2py/icepyx>
- 507 Stroeve, J. C., Jenouvrier, S., Campbell, G. G., Barbraud, C., & Delord, K. (2016).
508 Mapping and assessing variability in the antarctic marginal ice zone, pack ice
509 and coastal polynyas in two sea ice algorithms with implications on breeding
510 success of snow petrels. *The Cryosphere*, *10*(4), 1823–1843.
- 511

- 512 Tagliabue, A., & Arrigo, K. R. (2006). Processes governing the supply of iron to
513 phytoplankton in stratified seas. *Journal of Geophysical Research: Oceans*,
514 *111*(C6).
- 515 Vignon, É., Roussel, M.-L., Gorodetskaya, I., Genthon, C., & Berne, A. (2021).
516 Present and future of rainfall in antarctica. *Geophysical Research Letters*,
517 *48*(8), e2020GL092281.
- 518 Wang, S., Bailey, D., Lindsay, K., Moore, J., & Holland, M. (2014). Impact of sea
519 ice on the marine iron cycle and phytoplankton productivity. *Biogeosciences*,
520 *11*(17), 4713–4731.
- 521 Yoshida, K., Seger, A., Kennedy, F., McMinn, A., & Suzuki, K. (2020). Freezing,
522 melting, and light stress on the photophysiology of ice algae: ex situ incuba-
523 tion of the ice algal diatom *fragilariopsis cylindrus* (bacillariophyceae) using an
524 ice tank. *Journal of Phycology*, *56*(5), 1323–1338.